ELSEVIER

Applied Surface Science 154–155 (2000) 345–352

applied surface science

www.elsevier.nl/locate/apsusc

Strategy of nanocluster and nanostructure synthesis by conventional pulsed laser ablation

W. Marine [a,*], L. Patrone [a], B. Luk'yanchuk [b], M. Sentis [a]

[a] *Groupement Interdisciplinaire Ablation Laser et Applications, UMR CNRS 6631 and UMR CNRS 6594, Faculté des Sciences de Luminy, Case 901, 13288 Marseille Cedex 9, France*

[b] *General Physics Institute, Russian Academy of Sciences, 117942 Moscow, Russia*

Received 6 June 1999; accepted 21 July 1999

Abstract

We describe the basic principles of nanoparticle synthesis by conventional pulsed laser ablation. The generalization of the Zeldovich and Raizer theory of condensation has been performed for inhomogeneous laser-induced plume where the rates of nucleation as well as the condensation times are different for different parts of the plume. The theoretical development and analysis of the experimental results are given for condensation, expansion and properties of silicon nanoclusters.

Keywords: Laser ablation; Silicon clusters; Nanocrystals; Theory of condensation; Photoluminescence

1. Introduction

In this paper, we describe the basic principles of nanocluster synthesis by conventional pulsed laser ablation (PLA). Clusters are aggregates of atoms, or molecules, with a typical size from some tens up to a few thousands of atoms.[1] The small dimensions of these particles determine their properties strongly characterized by quantum effects. The properties of large clusters of 10–20 nm approach those of the corresponding bulk materials.

Nanometer-sized semiconductor particles proved to be a very promising material, since quantum confinement in such structures modifies the bulk Si band structure and results in radiative transitions. The elemental semiconductor nanocrystals Si and Ge at room temperature exhibit visible light emission at energies greater than the band gap of the bulk semiconductors. An efficient photoluminescence from the blue to the infrared has been reported from Si, oxidized Si and Ge nanoparticles.

In most of the previous laboratory experiments, nanoclusters were produced using a PLA supersonic expansion source of the Smalley type [2] or one of its modifications. For this source, collisions between monoatomic particles and the expanding high-pressure gas (generally He at pressure of about 1–10 atm), cool the particles and allow a heterogeneous nucleation and the growth of the clusters. However, this technique produces a relatively broad cluster size distribution.

An alternative method of nanocluster synthesis is the conventional PLA. In this case, ablation is per-

* Corresponding author. Tel.: +33-4-918-291-73, fax: +33-4-918-291-76.

E-mail address: marine@gpec.univ-mrs.fr (W. Marine).

[1] See, for example, Ref. [1] and references therein.

0169-4332/00/$ - see front matter
PII: S0169-4332(99)00450-X

formed at relatively low gas pressure, 0.2–10 Torr, of inert or reactive gas. During expansion and cooling, condensation starts within the ablated vapor and the condensed particles undergo multiple collisions with ambient gas molecules, leading to the stabilization of the nanoclusters before they arrive to the substrate surface. The size of the nanoclusters can be controlled by the laser parameters: fluence, wavelength, pulse duration and by the ambient gas conditions: pressure, nature and flow parameters.

Condensation of nanoparticles within the laser-induced vapor plume is a common phenomenon in PLA and was observed in numerous pulsed laser deposition (PLD) experiments. For more details, see, for example, the review by Chen [3] and references therein. The first synthesis of Si-based nanocluster films by conventional PLA has been reported by Movtchan et al. [4] and further development has been described in Refs. [5,6]. Motivated by the importance of the Si nanocluster synthesis, a number of groups reproduced these results [7,8], and the first fabrication of electroluminescent diodes of Si nanoclusters by PLD has been reported by Yoshida and Yamada [9]. Geohegan et al. have recently published new results on the dynamics of Si nanocluster formation [10] by PLA and on the luminescence of free, gas phase Si nanoclusters [11].

This new, rapidly growing, area of application of conventional PLA and PLD started with the synthesis of Si nanoclusters and is expanding towards the synthesis of clusters of compound materials [12,13], of oxides [14] and metals [15,16]. In this paper, we describe the basic principle of nanocluster condensation and present recent experimental results on the Si nanocluster synthesis.

2. Condensation of vapor and nanocluster formation

An idealized scheme of the cluster film synthesis by PLA can be separated into four independent steps: cluster nucleation, growth, cluster cooling and deposition.

(i) The nucleation is determined by the thermodynamic parameters of the material and by the initial conditions, like temperature and density of the vapor ejected after PLA. The nucleation process is characterized by the condensation temperature which can be found from general thermodynamic considerations.

(ii) The cluster growth will occur only during the collisional expansion between the ablated particles; thus, the main process determining the growth will be the plume expansion dynamics. The expansion dynamics can be strongly influenced by ambient gas effects such as the plume confinement due to collisions between the ablated particles and gas molecules.

(iii) Clusters are generally generated with a large amount of internal energy in liquid-like or solid-like states. The main paths of cluster stabilization are radiative, evaporative and collisional cooling. The first two mechanisms are evidently dominant in plume expansion under vacuum and the last one is present during the diffusive expansion of the plume into the ambient gas. The efficiency of collisional cooling will strongly depend on the temperature and density of the ambient gas determined by the hydrodynamics of the plume expansion.

(iv) The critical parameter of deposition of free clusters on a substrate is the kinetic energy (E) per atom in a free cluster of N atoms. Roughly, if E/N is less than the binding energy, one could expect the deposition of free clusters without fragmentation and structural rearrangement on the substrate. In the opposite case, the energy of the impact may be high enough to melt or to evaporate the clusters. Thus, strong deceleration of clusters is a necessary condition for cluster deposition.

In all steps of cluster formation mentioned above, the main process influencing the cluster evolution is the plume expansion dynamics. An accurate description of the plume expansion into vacuum can be made on the basis of the special solution of the gas dynamics equations given by Anisimov et al. [17]. From this solution, we found the following law for the isentropic expansion of spherical plume with radius $R(t)$ [18]:

$$\left(\frac{R(t)}{R_0}\right)^2 = \Psi(t) = 1 + 2\frac{u_0}{R_0}t + \left[\left(\frac{u_0}{R_0}\right)^2 + \frac{16}{3}\frac{E}{MR_0^2}\right]t^2, \qquad (1)$$

where R_0 and u_0 are the initial radius and velocity of the plume expansion, E is the initial internal energy and M is the total mass of the vapor. This solution holds for a monoatomic gas with adiabatic exponent $\gamma = c_p/c_v = 5/3$.

We use this solution to describe the density, specific volume, pressure and temperature profiles within the plume during its expansion. We consider that small droplets of condensed vapor *move together with the vapor* and we assume that the condensation process does not change the expansion dynamics of the plume. In this case, the different condensation phenomena can be described independently for each fixed Lagrangian coordinate $\xi = r/R(t)$. For arbitrary value of ξ, one can express the change of specific volume V in the following form:

$$\frac{1}{V}\frac{dV}{dt} = \frac{3}{2}\frac{1}{\Psi}\frac{d\Psi}{dt}. \quad (2)$$

For the analysis of the cluster formation process, we use the Zeldovich–Raizer (ZR) theory of condensation [19,20]. The condensation process starts when the plume becomes saturated and stops when the plume starts to expand in the collisionless (free-flight) regime. Within the inhomogeneous plume, saturation and free-flight regimes are reached for each point at different instant, that is, the saturation and the quenching waves propagate through the expanding vapor.

Before the start of condensation, the expansion of the plume occurs along the Poisson adiabat, PV^{γ}. The expansion continues until the Poisson adiabat intersects the saturated vapor adiabat given by the Clapeyron–Clausius equation. The condensation starts at the moment $t = t_c$ when the vapor is cooled down to the condensation temperature $T = T_c$. It should be noted that T_c does not depend on the coordinate ξ, that is, we obtain the same condensation temperature for different parts of the plume. However, the time t_c at which condensation starts depends on coordinate ξ, that is, the different parts of the plume start to condense at different times. The plot of the saturation wave is shown in Fig. 1. It can be seen that the saturation wave propagates through the plume from the periphery to the center. We note that the part of the plume with $r > 0.6R_0$ is already situated within the region of saturation at $t = 0$. For example, shown in Fig. 1, $u_0 = 6 \times 10^5$ cm/s, the saturation wave reaches the point $r = 0$ (i.e., the whole plume becomes saturated) at the time $t = 40$ ns.

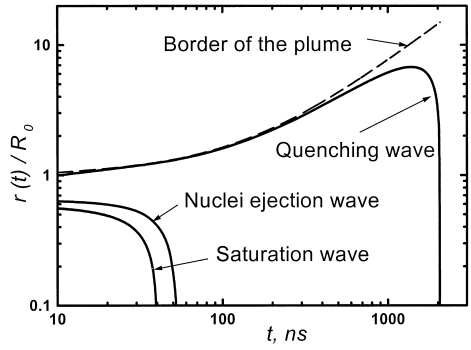

Fig. 1. Propagation of saturation, quenching and 'ejection' waves through the Si vapor plume. Initial parameters of the plume: velocity 6×10^5 cm/s, radius 0.1 cm, specific volume 300 cm^3/g, temperature 7000 K, pressure 68.4 atm.

The time when the condensation stops is determined by a ''quenching effect''. It occurs at some stage of the expansion (for more detail, see Refs. [18,21]), when the collisions within the expanding vapor become negligible. We shall give a simple estimation of this quenching time. To find the boundary $r = r_q(t)$ between the collision (hydrodynamic) and collisionless (free-flight) regions of the plume, we use the criterion $\ell \nabla v = v_s$. Here, $\ell = 1/\sigma_g N$ is the mean free path within the hydrodynamic region. Where σ_g is the collisional cross-section, N is the vapor concentration and v_s is the velocity of sound at the given point. The meaning of this criterion is rather simple: in the hydrodynamic (collisional) regime, the change of velocity over the mean free path λ is much less than the sound velocity (i.e., the mean molecular velocity).

The propagation of quenching waves through the plume and the border of the expanding plume are shown in Fig. 1. It can be seen from the figure that the linear stage of the plume expansion starts around 700 ns. Thus, all important events within the plume occur during the nonlinear stage of the expansion. Our calculations show the strong influence of the initial velocity u_0 on the quenching process. The whole plume becomes collisionless at $t = 2071$ ns with $u_0 = 6 \times 10^5$ cm/s (Fig. 1) and at $t = 5963$ ns when $u_0 = 0$.

The third wave shown in Fig. 1 refers to the trajectory which delivers the maximum of supersaturation. Under these conditions, the nuclei are formed (''ejected'' into the saturated vapor).

In this part of our paper, we have introduced the dynamics of condensation and cluster formation. We discussed the propagation of the nucleation wave (starting point of condensation) and the propagation of the quenching wave, where the condensation and growth stop. From this analysis, we delimit the time scale of these two processes which can be tested experimentally by time-resolved measurements.

The solution of the nuclei growth problem takes into account the thermodynamics of the two-phase (liquid + vapor) region and the kinetics of condensation during the plume expansion. Our analysis is based on the Zeldovich's kinetic equation [19] and can be found in Ref. [18].

One of the results of this analysis is shown in Fig. 2, which illustrates the dependencies of the cluster size on plume temperature T_0 and initial density ρ_0. One can see from the calculations that the cluster size falls down with the increasing temperature (at fixed specific volume). However, it is not easy to change these conditions experimentally, for example, by a variation of the laser parameters. Indeed, while an increase of the laser fluence increases the initial temperature T_0, it simultaneously increases the initial density, that is, a compensation effect takes place. Thus, to investigate the optimal laser control of the cluster formation, one should solve the laser ablation problem (find parameters T_0, ρ_0, etc.) in combination with the hydrodynamics of the condensation problem.

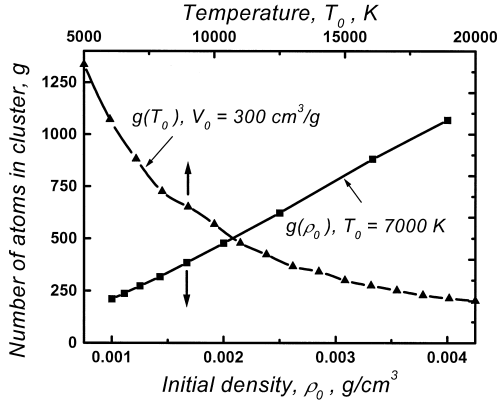

Fig. 2. Number of atoms within the cluster versus temperature and density.

During ablation into gas, the nucleation stage may be analyzed in a similar way. However, this analysis may only be applied to the very early expansion stage, when the collisions of the ablated particles with the ambient gas affect only the leading edge of the plume. Thus, to find the optimal laser control for cluster formation, one should solve a set of hydrodynamics equations for the plume expansion into the ambient gas taking into account the dynamics of vapor condensation. While the numerical modeling of the plume expansion is well in progress [22–25], the problem of nanocluster condensation in the presence of buffer gas is not yet solved and represents a challenge for future PLA developments.

3. Experimental results

A survey of the published experimental results shows that clusters formed from the vapor phase, typically in the nanometer range, are much smaller than the well-known droplets (0.1 to 5–10 μm) produced by melt ejection from a target [3]. The size of nanoclusters can be controlled by the ambient gas pressure, whereas the largest particles are essentially the same in vacuum or in a gaseous ambient.

At present, the best documented material is Si. Due to its important technological applications, several laboratories have studied the dynamics of Si nanoparticles formation. The question is where and when the Si nanoparticles collected on the substrate were formed and how to optimize the rate of synthesis and the collection of the gas-formed nanoclusters.

One of the first attempts to analyze the Si cluster emission in vacuum after PLA has been made by Kasuya and Nishina [26]. They observed a direct emission of Si^+ and Si_2^+ after nitrogen laser excitation (photon energy $h\nu = 3.68$ eV, pulse duration $\tau = 10$ ns, fluence $F = 2$ J/cm^2). They show that charged clusters with $M/q = 1.25$–1.5 (where M is the number of atoms and q is the charge) are formed during the first 100 ns after the end of the laser pulse. During expansion into vacuum, the parent clusters decompose mostly into individual ions

through numerous channels of fragmentation on a time scale of 10 μs. Okano and Takayanagi [27]. reported observation of small neutral Si_n clusters ($n = 2$–11) produced by YAG laser irradiation in vacuum. In this experiment, it was observed that the clusters become present in the plume at a time delay of about 100 ns and at a distance of less than 1 mm from the target. Vijayalakshmi et al. [28] used extremely low laser fluence, $F = 191$ mJ/cm^2 (KrF laser, $h\nu = 5$ eV, $\tau = 8$ ns) for vacuum ($P = 8 \times 10^{-6}$ Torr) deposition of Si nanoclusters. From atomic force microscopy (AFM) measurements, the average cluster size was found to be about 25 nm for the target–substrate distance of $D = 3$cm. However, micro-Raman scattering experiments indicated a cluster size of 4–5 nm. The authors also mentioned that the cluster size decreased with increasing D. Movtchan et al. [5] used optical time of flight (TOF) spectroscopy and reported cluster luminescence with a delay of $\Delta t = 0.1$–5 μs after ArF laser ablation ($h\nu = 6.4$ eV, $\tau = 15$ ns, $F = 2$ J/cm^2). In this experiment, Si cluster luminescence was observed in vacuum and in gases (He, Ar, O_2) at low pressure (0.2–1 Torr). The cluster size, estimated from the TOF spectra was about 26–40 atoms. This estimation was confirmed by AFM and by a comparison of the observed emission spectra with absorption spectra of size-selected Si_n clusters ($n = 18$–41).

The main conclusion from these experiments is that Si_n nanoclusters ($n = 2$–40) are formed, either in vacuum or in a buffer gas at low pressure, on a time scale of about 100 ns. All these observations are in good agreement with our calculation of the time of cluster condensation and nuclei ejection into saturated vapor.

As mentioned above, the introduction of a buffer gas during PLA leads to a confinement of the plume and a deceleration of the ablated particles. The confinement results in a decrease of the cooling rate of the plume.

In recent experiments, Muramoto et al. [29] and Geohegan et al. [10,11] used time-resolved optical imaging of gas phase Si nanoparticles excited by an external laser. In these studies, high pressure (5–10 Torr) of the ambient gas (He) and relatively high fluence, $F = 4$–10 J/cm^2 of KrF laser ($h\nu = 5$ eV, $\tau = 28$ ns), were used. In both experiments, the delay time of the onset of the cluster observation was about 150–200 μs. The quasi-simultaneous observation of the Rayleigh scattering (RS) and photoluminescence signals (PL) [10,11] shows the presence of well-formed relatively cold solid Si clusters. Muramoto et al. determined the clustering reaction as a formation of Si_2 molecule with following cluster growth. According to our theoretical development (see, for example, Fig. 1), the formation of nanoclusters is completed at the beginning of the quenching, that is, the time when the collisions between ablated particles are terminated. For typical conditions of the expansion into vacuum, this time is about 2 μs. During the plume expansion into the ambient gas, it must be larger (6–20 μs, depending on the initial conditions and the gas pressure), due to the confinement of the plume. The origin of the delayed PL and RS in Ref. [10] can be explained by the following fact. The temperature of nanoparticles at the moment of quenching is still high, about 2000–2500 K, the clusters at this temperature are small (1.5–3 nm) liquid particles [18]. Recently, we have shown that the observed delay time of PL is related to the long stage of the evaporative and collisional cooling and to the cluster crystallization [30]. Both PL and RS signals appear at sufficiently low temperature, when the phase transition, liquid–solid, and structural transitions of the nanoparticles are completed. These calculations are in a very good agreement with the temperature measurements of Si atoms by Le et al. [31]. The temperature of Si atoms has been determined from the Doppler broadening of the Si ($3d\ ^1p^0$–$3p^2\ ^1s$) transition. From these results, it can be seen, that at the delay of 5 μs, the temperature of Si atoms in Ar gas is higher than the melting temperature (T_m) of bulk Si and near T_m in the case of ablation into He ambient gas. The stabilization of Si nanoclusters, which have probably a lower T_m [32] than bulk Si, is completed after approximately 100–300 μs and 1–3 ms in He and Ar gases, respectively.

Several groups reported on the determination of the Si nanocluster size as a function of the pressure of the inert ambient gas. Yoshida et al. [33] have shown that the diameter (10–20 nm) of Si particles is proportional to $P^{1/2.8}$ power of the He gas pressure. Makimura et al. [8] used the second harmonics of a Nd:YAG laser ($h\nu = 2.34$ eV, $F = 10$ J/cm^2) and found that the Si nanoparticle diameter vary with

$P^{1/1.3}$ for $P = 0.5$–20 Torr of He gas. Lowndes et al. [12] carefully reproduced the experiment of Yoshida et al. [33] and showed that, for the target–substrate separation between 10–40 mm, the mean Si nanocluster size was maximized for $P \cong 6$ Torr. In these experiments, large nanoclusters (0.8–7 nm) were deposited on the substrate close (10 mm) to the target. For larger D, the size distribution shifted towards smaller dimensions; 0.2–0.8 nm particles have been collected at $D = 40$ mm. The existence of a maximum in the size distribution versus He pressure is in striking contrast to the results of Refs. [8,33]. A similar dependence, with a maximum of the size distribution as a function of ambient gas pressure (Ar, He), was also observed by Deleval [34].

An alternative method of cluster deposition uses the backward flux of the ablated particles [4–6]. A backward-propagating flux of ablated particles was observed in several experiments by TOF spectroscopy [10], by rapid imaging of the plume expansion [5,10,35], and was predicted by numerical calculations of the plume expansion dynamics into low pressure gases [24,25,36]. At high gas pressure (1 atm), this flux is connected to the well-known effect of debris deposition [37]. In the backward deposition setup, the substrate for deposition is located near the laser spot, in parallel to the small c-Si target.

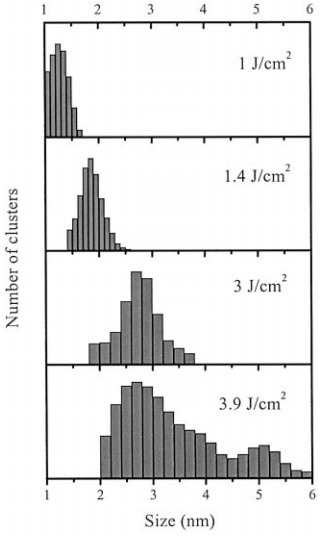

Fig. 3. Si cluster size distribution for deposits prepared at 4 Torr of He and at different laser fluence.

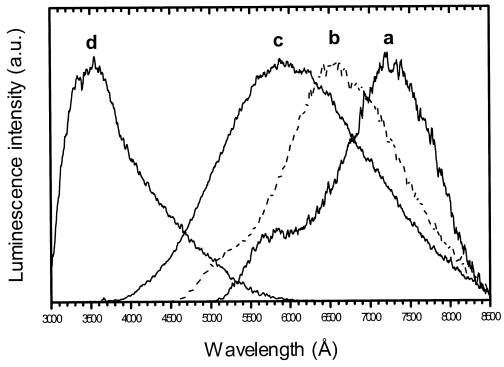

Fig. 4. Photoluminescence spectra of Si nanoclusters. Samples were prepared under 4 Torr of He at different fluences: (a) 3.9 J/cm^2, (b) 3 J/cm^2, (c) 1.4 J/cm^2, (d) 1 J/cm^2. The excitation photon energy was 4.8 eV. The spectral intensities are normalized.

In Fig. 3, we show the size distribution of the Si nanoclusters versus the fluence of an ArF laser ($\tau =$ 15 ns). In this case, we used the backward geometry of deposition, with a He pressure of 4 Torr. The size selection was performed by careful variation of the synthesis parameters. Fig. 4 shows the PL spectra corresponding to the size distributions of Fig. 3. From these figures, it can be seen that the size selection of Si_n clusters allows one to tune the PL bands within a large spectral region ranging from near UV to near IR. The observed size-dependent PL supports the quantum confinement model of electronic properties of Si nanoclusters .

In the early experiments [4,6–8], the synthesis of Si and Si–SiO_x nanocluster films by conventional PLA or by supersonic expansion methods [38,39] did not reveal any significant size dependence of their properties. This was probably due to a very large size dispersion of the nanoclusters on the substrate and/or cluster coalescence during deposition or after a high-temperature annealing [8,39]. Recently, Patrone et al. [40] showed that Si nanoclusters prepared by backward PLA deposition exhibit quite reproductive properties.

4. Conclusion

In this paper, we introduced the basic principles of nanocluster synthesis by conventional PLA. We

showed that, for clusters moving together with the vapor, one can distinguish three different waves propagating through the plume: (1) the wave of saturation (where the vapor becomes saturated), (2) the supercooling wave where the highest supercooling is reached, and (3) the quenching wave where the growth stops. After the condensation and the growth stages, the clusters follow a long stabilization period. The main channels of cluster stabilization are radiative, evaporative and collisional cooling. The typical time scales for these processes are 0.05–20 μs and 0.2–6 ms for the condensation-growth and cooling, respectively. Thus, depending on the deposition geometry (substrate–target distance, substrate position), the nanostructured deposit will be formed from liquid, hot solid or well-stabilized gas-phase nanoclusters. The quality of the nanocluster structure will depend on the secondary processes occurring on the surface such as nanocluster coalescence and enhanced mobility. These two processes play an important role during the deposition of relatively hot clusters.

Our general description of nanocluster synthesis is valid for all systems: semiconductors, metals and oxides. However, a significant modification of this approach must be introduced for heterogeneous systems where a large number of precursors of condensation (small clusters, charged atoms and molecules) are present at the early stage ($\sim$100 ns) of the plume expansion.

From the experimental point of view, stable and reproducible synthesis of Si nanoclusters, with the ability to vary their size, passivation and doping, is a significant processing advantage of the PLA technique, which is compatible with ultrahigh vacuum and reactive deposition environments.

References

[1] H. Haberland (Ed.), Clusters of Atoms and Molecules, Springer-Verlag, 1994.
[2] J.R. Heath, Y. Liu, S.C. O'Brien, Q.L. Zhang, R.F. Curl, F.K. Tittel, R.E. Smalley, J. Chem. Phys. 83 (1985) 5520.
[3] L.C. Chen, in: D.B. Chrisey, G.K. Hubler (Eds.), Pulsed Laser Deposition of Thin Films, Wiley, 1994, p. 195.
[4] I.A. Movtchan, R.W. Dreyfus, W. Marine, M. Sentis, M. Autric, G. Le Lay, N. Merk, Thin Solid Films 255 (1995) 286–289.
[5] I.A. Movtchan, W. Marine, R.W. Dreyfus, H.C. Le, M. Sentis, M. Autric, Appl. Surf. Sci. 96–98 (1996) 251.
[6] W. Marine, I. Movtchan, A.S. Simakine, L. Patrone, R.W. Dreyfus, M. Sentis, M. Autric, N. Merk, in: D. Singh, L. Norton, J. Laude, J. Narayan (Eds.), MRS Symposium Proceedings, Pittsburgh, 397 (1996) 365.
[7] Y. Yamada, T. Orii, I. Umezu, S. Takeyama, T. Yoshida, Jpn. J. Appl. Phys., Part 1 35 (1996) 1361.
[8] T. Makimura, Y. Kunii, K. Murakami, Jpn. J. Appl. Phys., Part 1 35 (1996) 4780.
[9] T. Yoshida, Y. Yamada, J. Appl. Phys. 83 (1998) 5427.
[10] D.B. Geohegan, A.A. Puretzky, G. Duscher, S.J. Pennycook, Appl. Phys. Lett. 72 (1998) 2987.
[11] D.B. Geohegan, A.A. Puretzky, G. Duscher, S.J. Pennycook, Appl. Phys. Lett. 73 (1998) 371.
[12] D.H. Lowndes, C.M. Rouleau, T. Thundat, G. Duscher, E.A. Kenik, S.J. Pennycook, Appl. Surf. Sci. 127–129 (1998) 355.
[13] J.M. Fitz-Gerald, T.A. Trottier, R.K. Singh, P.H. Holloway, Appl. Phys. Lett. 72 (1998) 1838.
[14] J.K. Gibson, J. Appl. Phys. 78 (1995) 1274.
[15] J.M. Ballsteros, R. Serna, J. Solis, C.N. Afonso, A.K. Petford-Long, D.H. Osborne, R.F. Haglund Jr., Appl. Phys. Lett. 71 (1997) 2445.
[16] Z. Pasti, Z.E. Horvath, G. Peto, A. Karacs, L. Guczi, Appl. Surf. Sci. 109–110 (1997) 67.
[17] S. Anisimov, D. Bauerle, B. Lyk'yanchuk, Phys. Rev. B 48 (1993) 12076.
[18] B. Lyk'yachuk, W. Marine, S. Anisimov, Laser Physics 8 (1998) 291.
[19] Y.B. Zeldovich, Sov. Phys. JETP 12 (1942) 525.
[20] Y.P. Raizer, Sov. Phys. JETP 37 (1960) 1229.
[21] Y.B. Zeldovich, Y.P. Raizer, Physics of Shock Waves and High Temperature Hydrodynamics Phenomena, Academic Press, NY, 1966.
[22] K.P. Chen, J.N. Leboeuf, R.F. Wood, D.B. Geohegan, J.M. Donato, C.L. Liu, A.A. Puretzky, Phys. Rev. Lett. 75 (1995) 4706.
[23] J.N. Leboeuf, K.P. Chen, J.M. Donato, D.B. Geohegan, C.L. Liu, A.A. Puretzky, R.F. Wood, Phys. Plasmas 3 (1996) 2203.
[24] H.C. Le, D. Zeitoun, Y. Burtschell, W. Marine, M. Sentis, R.W. Dreyfus, in: R. Singh, D. Norton, L. Laude, J. Narayan, J. Cheung (Eds.), MRS Symposium Proceedings, Pittsburgh, 397 (1996) 75.
[25] H.C. Le, PhD Thesis, Université de la Méditerranée, Marseille, France, 1997.
[26] A. Kasuya, Y. Nishina, Phys. Rev. Lett. 57 (1986) 755.
[27] A. Okano, K. Takayanagi, Appl. Surf. Sci. 127–129 (1998) 362.
[28] S. Vijayalakshmi, M.A. George, J. Sturmann, H. Grebel, Appl. Surf. Sci. 127–129 (1998) 378.
[29] J. Muramoto, Y. Nakata, T. Okada, M. Maeda, Jpn. J. Appl. Phys., Part 2 36 (1997) L563.
[30] B. Luk'yanchuk, W. Marine, Appl. Surf. Sci. 154–155 (2000) 31.
[31] H.C. Le, R.W. Dreyfus, W. Marine, M. Sentis, I.A. Movtchan, Appl. Surf. Sci. 96–98 (1996) 164.

[32] Y. Leereah, G. Deutscher, P. Cheyssac, R. Kofman, Europhys. Lett. 12 (1990) 709.
[33] T. Yoshida, Y.S. Takeyama, Y. Yamada, K. Mutoh, Appl. Phys. Lett. 68 (1996) 1772.
[34] S. Deleval, DEA Thesis, L'Univesité Aix-Marseille I, 1996.
[35] K. Scott, J.M. Hantley, W.A. Phillips, J. Clarke, J.E. Field, Appl. Phys. Lett. 57 (1990) 922.
[36] T. Itina, W. Marine, M. Autric, J. Appl. Phys. 92 (1997) 3536.
[37] A. Miotello, R. Kelly, B. Braren, C.E. Otis, Appl. Phys. Lett. 61 (1992) 2784.
[38] E. Werwa, K.D. Kolenbrander, in: R. Singh, D. Norton, L. Laude, J. Narayan, J. Cheung (Eds.), MRS Symposium Proceedings, Pittsburgh, 397 (1996) 381.
[39] E. Werwa, A.A. Seraphin, L.A. Chiu, C. Zhou, K.D. Kolenbrander, Appl. Phys. Lett. 64 (1994) 1821.
[40] L. Patrone, D. Nelson, V.I. Safarov, M. Sentis, W. Marine, J. Lumin. 80 (1999) 217.